Analysis of the Impact of Artificial Networks in System-level EMC Tests

Pablo J. Gardella
Allegro MicroSystems Argentina
Instituto Tecnológico de Buenos Aires (ITBA)
CABA, Argentina
pgardella@allegromicro.com
pgardell@itba.edu.ar

Eduardo Mariani
Allegro MicroSystems Argentina
EM Ingeniería
CABA, Argentina
emariani.cw@allegromicro.com

***Abstract*—The impedance of an Off-The-Shelf Artificial Network (OTS-AN) and a custom made High-Frequency Artificial Network (HF-AN) were analysed and compared. It is showed that in order to meet the requirements of automotive standards, such as Bulk Current Injection (BCI) from ISO 11452-4 as well as both Conducted and Radiated Emissions (CE, RE) from CISPR 25, the HF-AN is needed. System-level circuit simulations were run using S-parameters for quantifying the impact of these two models in the previously mentioned EMC tests. Above 50 MHz, up to 3.5 dB and 4.3 dB differences were found on the transfer-impedance of CE and in the Common-Mode to Differential-Mode conversion of BCI, respectively. On the other hand, in RE the OTS-AN leaded to an overestimation of the emission profile in the 300 MHz and 800 MHz band as high as 5.3 dB. Besides that, it is showed that the OTS-AN behaves as a source of non-constant uncertainty, specially above 50 MHz. Finally, the issues in terms of reproducibility, repeatability and accuracy that arise from the non-RF connectors in the OTS-AN are discussed and a metric for test-bench comparison and validation is proposed.**

***Index Terms*—Automotive EMC, Artificial Network, RF Immunity, RF Emissions, Bulk Current Injection (BCI), Radiated Emissions (RE), Conducted Emissions (CE), ISO 11452, CISPR 25**

I. Introduction

In recent years, ElectroMagnetic Compatibility (EMC) has become substantially important in the semiconductor industry, in particular in the automotive market. The developments towards the Electric Vehicle (EV), the Hybrid Electric Vehicle (HEV) and the Advanced Driver Assistance Systems (ADAS), among many others, are increasingly demanding stringent requirements in terms of EMC.

These requirements are usually called Final Compliance tests because they are performed at the Vehicle-level prior to market release. Nevertheless, automotive companies need to know in advance that the product they are currently designing is going to meet these tests once it is fully assembled. Therefore, they request from their suppliers, the autopartists, to comply with some System-level EMC tests usually known as Pre-compliance tests like Bulk Current Injection (BCI) [1], Conducted Emissions (CE) and Radiated Emissions (RE) [2].

In addition to that, the complexity of nowadays systems forces autopartists to have their own suppliers: the IC manufacturers. These ICs must go under other type of EMC tests, called IC-level tests, like Direct Power Injection (DPI) [3] and the Direct Coupling Method (DCM) [4]. These tests should correlate with the System-level tests and, at end of the process, with the particular Vehicle-level test demanded by the automotive company.

One of the main objectives of System-level tests, is to mimic the Vehicle-level by providing, for example, harness resonances and load circuits similar to the ones that will be employed by the Engine Control Unit (ECU) to communicate with the ICs in the application. Therefore, as proposed in [5], for the System-to-IC translation it becomes crucial to have accurate models of the test setups to simulate them at early stages. This methodology minimizes the risks associated with expensive and belatedly redesigns that may prevent to accomplish the expected times-to-market.

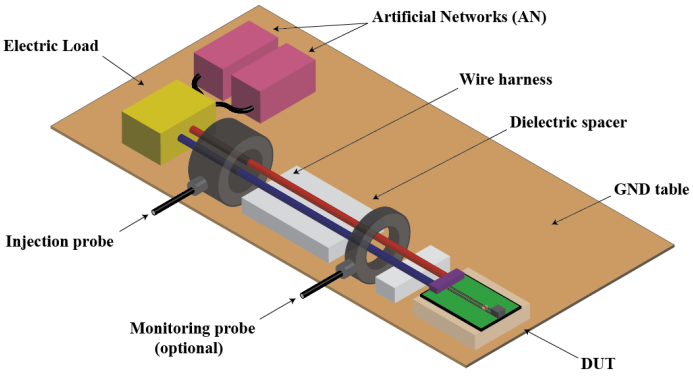

Fig. 1: Schematic representation of a typical closed-loop BCI test setup in a 2-wire harness. The figure is not to scale.

In regard to EMC modelling, the test setups are typically modelled by a divide-and-conquer strategy like the one showed in [6], [7] for BCI and in [8] for RE. The test setups can be splitted in common elementary blocks which not only reduces the computational time and memory requirements for ElectroMagnetic (EM) simulations or Network Analyser measurements, but also maximizes reusability across DUTs, test setup variations and also EMC tests.

Despite the modelling of the fundamental blocks has been extensively and deeply studied by many groups [5]–[10], the

study of the Artificial Networks (AN) and its impact on the test results has been focused on CE [11], [12] rather than on the full set of EMC tests. Also, as showed in [13], [14], the impact of the Battery Management System (BMS) on these tests is crucial in EV and HEV. However, in this regard there are essentially two type of situations based on the battery location: on the one hand, there are systems in which the power supply is provided through the AN, and there are others that require the DUT to be locally powered. This work will cover only the first situation in Low-Voltage (LV) and Low-Power (LP) applications. The second case is much more delicate as the battery and its State of Charge (SoC) will have a direct impact on the power transfer [15] and therefore an accurate modelling of its impedance is needed [15]–[17].

The real-world correlation of the System-level tests makes their modelling considerably challenging. Therefore, if the fundamental blocks are not precisely described, not only the accuracy and usefulness of the early-design simulations will get degraded, but also the inter-laboratory reproducibility. This work proposes to study the AN, aka Line Impedance Stabilization Network (LISN), and its impact on some of the most common System-level EMC tests, with special emphasis in real-life situations. This analysis is essential within the framework of IC-level requirements derivation, as they depend on an accurate System-level modelling for the aforementioned reasons [5].

In the first section, the different test setups and their building blocks will be described. Secondly, measurements of an Off-The-Shelf AN (OTS-AN) and a High-Frequency AN (HF-AN) will be presented with their corresponding impact on the System-level EMC tests under analysis, and finally the results will be discussed.

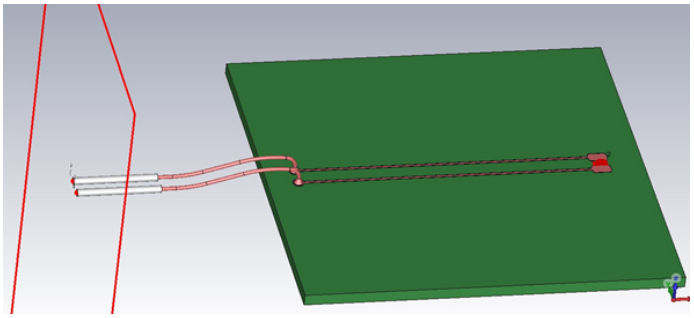

Fig. 2: EM model of the PCB for the 2-wire case. The perpendicular plane on the left indicates where the IC ports are, while the two pads on the right constitute the floating lumped port for the 2-pin IC.

II. System-level test setups

The tests which have been analysed are BCI as per ISO 11452-4 (2020) [1] and CE, RE as per CISPR-25 (2016) [2]. The analyses have been performed using a modular approach where the reference of each block is the system GND and the blocks have been expressed in terms of their S-parameters.

For simplicity, a 2-wire IC situation has been chosen, where the output magnitude to be acquired by the ECU is the supply current. This is accomplished by the use of an RC shunt composed of a 50 Ω resistor and a 1 nF capacitor (ESL = 1 nH, ESR = 0.1 Ω) as the Electric Load of the system. The DUT is considered to be composed by a 50 mm x 50 mm FR4 PCB with the layout showed in Fig. 2. EM simulations have been performed using CST Studio as the frequency domain solver with an input QTEM port for each wire [6]. The bottom layer is a GND plane connected to the GND pin at the input pads and the IC is supposed to be connected to lumped floating ports on the opposite side of the board.

A. Conducted Emissions (CE)

The CE setup analysed in this work corresponds to the voltage method test outlined in [2] (showed in Fig 3) with a 200 mm harness. For a 2-wire IC, the test can be conceptually simplified to the measurement of the voltage across the ANs' 50 Ω loads to infer the Icc spectrum (aka Normal Mode). Therefore the transfer-impedance between the IC's current and the AN's load is the critical parameter and was the metric for comparison between the different AN models. The two lines of the harness were referenced as POS, NEG after the IC polarity. This model has been obtained by EM simulations.

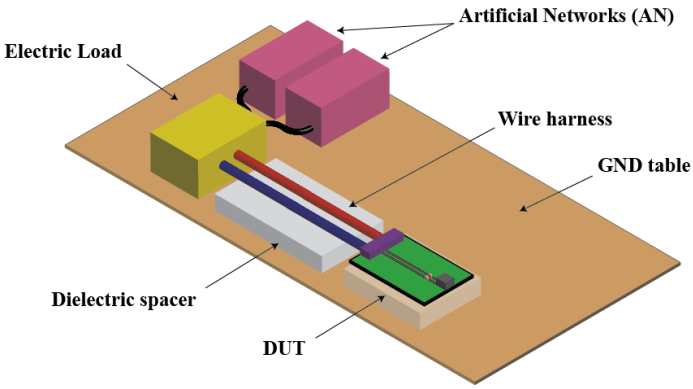

Fig. 3: Schematic representation of a typical CE test setup in a 2-wire harness. The figure is not to scale.

B. Bulk Current Injection (BCI)

The BCI test setup is showed in Fig 1 and consists on the lumped-element model of a field-to-wire coupling by using a ferrite-based transformer as an injection probe [18]. A secondary probe can be used for monitoring the effectively injected current in the wire harness and this situation is referred as the closed-loop BCI setup. During a test, the injection probe delivers some amount of Common-Mode (CM) disturbance to the wiring harness, in which it can leak into a Differential-Mode (DM) due to the unbalances of the test setup, and can eventually be delivered to the Device Under Test (DUT). As showed in [6], [7], this CM-to-DM conversion is one of the most critical parameters in BCI, since DUTs are susceptible to the DM rather than to the CM. In this work, the CM-to-DM conversion was the metric for comparison and it was inferred by the insertion loss between an input RF

generator and a differential 50Ω load connected across the IC pins.

In this work, a closed-loop 1000 mm length 2-wire harness with the injection probe at 900 mm and the monitoring probe FCC F-65 placed at 50 mm from the DUT were analysed. The 2-wire harness is the one showed in Fig 1 and it has been characterized with VNA measurements.

C. Radiated Emissions (RE)

The RE setup analysed in this work follows the Absorber Lined Shielded Enclosure (ALSE) method outlined in [2] and it is presented in Fig 4. For the EM simulation of the 1500 mm harness, a free-field environment was employed as an idealization of the enclosure by considering the direct-field from the harness only. Since the CM current along the harness is the main contributor to the electric field integrated by the antenna, it was chosen as the metric for comparison [19].

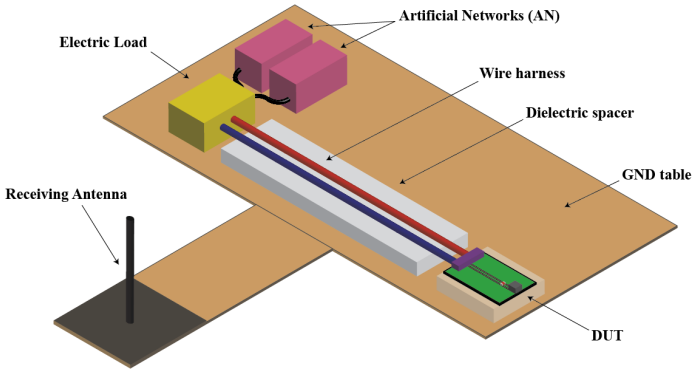

Fig. 4: Schematic representation of a typical RE test setup in a 2-wire harness with a monopole antenna as per CISPR 25 (2016) [2]. The figure is not to scale.

III. Artificial Network

The OTS-AN studied in this work is a 5 μH/50 Ω Schwarzbeck NNBM 8124-200N, which according to the manufacturer, is suitable for CISPR 25 and BCI testing. An example of a typical AN schematic proposed in [2] is showed in Fig 5 and a picture of the actual OTS-AN is showed in Fig 6. The electrical requirements are defined in CISPR 16-1-2 [20].

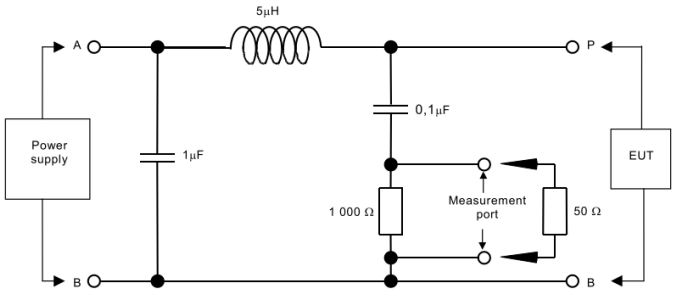

Fig. 5: Example of an AN circuit from CISPR 25 (2016) [2].

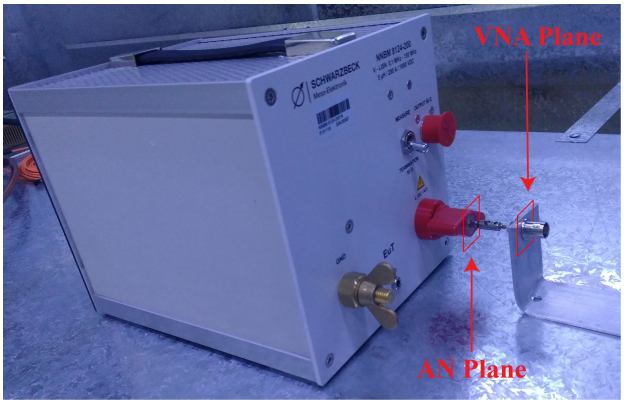

Fig. 6: Artificial Network with the VNA calibration plane and the shifted reference plane for the impedance definition.

In order to characterize the OTS-AN impedance up to 1 GHz, which is the maximum frequency needed in RE [2], a 1-port AN was defined. Subsequently, a 3-port system was defined where port 1 corresponds to the EUT of Fig 5, port 2 to the Power supply and port 3 to the 50 Ω load. Given the non-RF connectors of the OTS-AN under study, vertical fixtures were built as showed in [21], [22]. However, in contrast with those situations, this work develops a full 3-port model instead of a 1-port simplification. This allows the model to be used for CE simulations, where an RF receiver is connected to the 50 Ω port, also this model is convenient for quantification of the isolation between the DC and the RF side, which is important to guarantee independence of the battery impedance.

A. 1-port AN

In the first place, the reflection coefficient (ρ) of the OTS-AN was measured with the VNA between 1 MHz and 1 GHz. Then, the vertical structures employed in the process were de-embedded to obtain ρ'. However, as explained in [22] the standards do not define a reference plane and attribute the phase errors to the uncertainty budget. Besides that, since the banana jacks are not 50 Ω transmission lines, depending on the user's election the impedance can either be compliant or not with the requirements! In this work, the reference plane was defined at the outer edge of the input banana jack, as showed in Fig 6.

The de-embedding has been approximated by shifting the measurement plane from the vertical structure to the red connector in Fig 6 with the following equation:

$$\rho' = \rho \cdot e^{j\frac{2\pi f}{c}2L} \tag{1}$$

Where c is the speed of light in air, f is the frequency and L represents the distance between planes, which in this case is 45 mm. The factor of two comes from the fact that the wave travels the distance twice.

Even after performing the de-embedding, the OTS-AN is still not compliant with the requirement for BCI and RE. It is worth mentioning that the standards and the manufacturer only define the impedance up to 108 MHz, despite BCI goes up to 400 MHz and RE to 1 GHz.

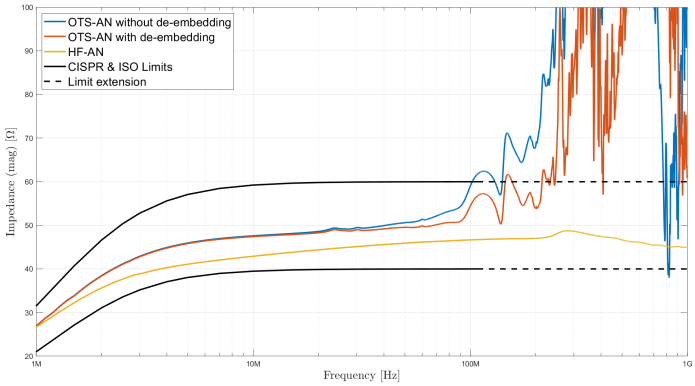

Fig. 7: 1-port AN impedance with battery port shorted.

As showed in Fig 7 and supported by [9], [10], the non-RF design of the OTS-AN introduces important differences in the impedance. However, if those differences were systematic they would not be much of an issue. The problem is the randomness introduced by the non-RF connectors from site-to-site. Despite that quantification is beyond the scope of this work, the single-case analysis of de-embedding 45 mm of an ideal transmission line is sufficient to perceive the significant uncertainty associated to single-line cables with lengths in the order of 150 mm. To overcome this problem, it was decided to build a HF-AN as the one proposed in [7] to meet the impedance requirement up to 1 GHz, while at the same time maximize the reproducibility of the tests in regard to the AN by using coaxial cables. The circuit is showed in Fig 8 and its input impedance have already been showed in Fig 7.

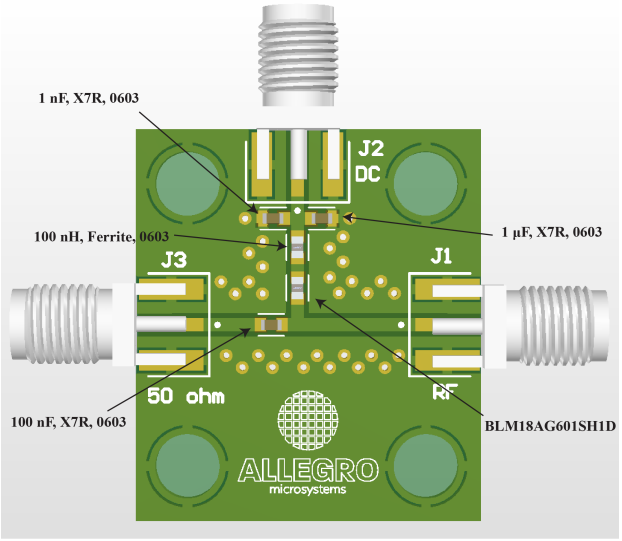

Fig. 8: HF-AN PCB design. The traces are 50 Ω Grounded CoPlanar Waveguides (GCPW) with via fences. A ferrite bead is used in the DC path prevent high-frequency resonances by taking advantage of its increasing resistance with frequency. The 100 nH inductor and the 1 nF capacitor guarantee the 40 dB isolation up to 1 GHz.

B. 3-port AN

After confirming the impedance compliance of the HF-AN, the 3x3 S-parameters matrix was measured across the same frequency range for analysing the other relevant magnitudes: isolation and coupling.

In terms of the isolation between the battery and the other ports, as showed in Fig 9, the HF-AN meets the 40 dB requirement of [20]. In regard to the coupling, a maximum difference of 1 dB was seen in the insertion loss within the CE frequency band (where the coupling is relevant).

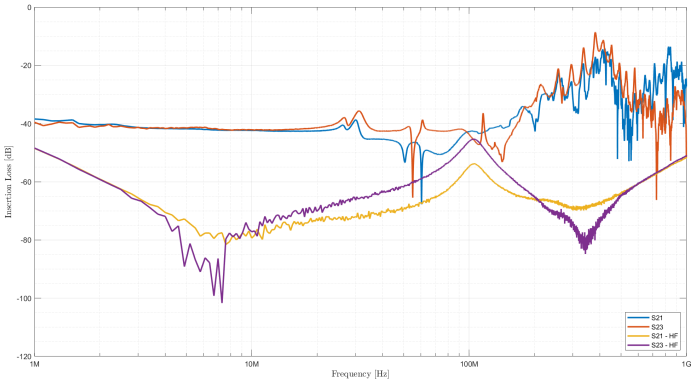

Fig. 9: Comparison of the AN insertion losses across the battery side (port 2) and both the RF side (port 1) and the 50 Ω load (port 3).

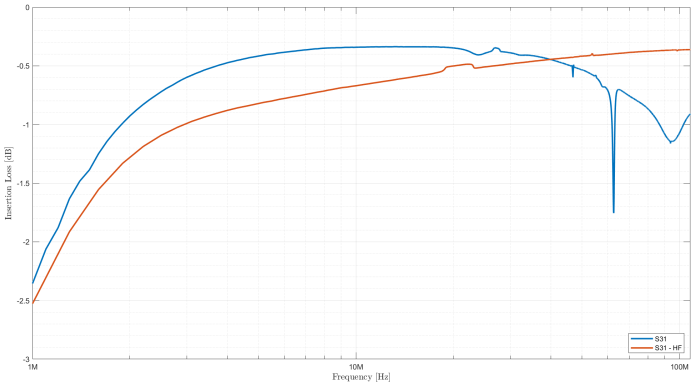

Fig. 10: Comparison of the AN insertion losses across the RF side (port 1) and the 50 Ω load (port 3).

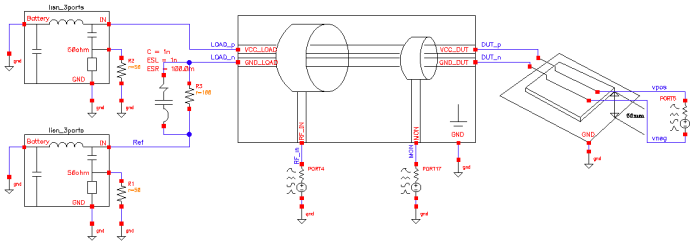

Fig. 11: Virtual environment for the 2-wire BCI simulation. For the CE and RE simulations, the harness was replaced by the corresponding block for each situation.

IV. System-level EMC simulations

All S-parameters, have been incorporated as Touchstone files into the System-level circuit simulation developed in the Cadence simulator showed in Fig 11.

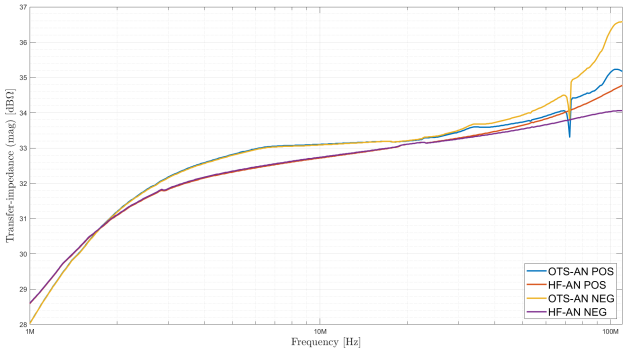

Fig. 12: Transfer-impedance in the CE simulation.

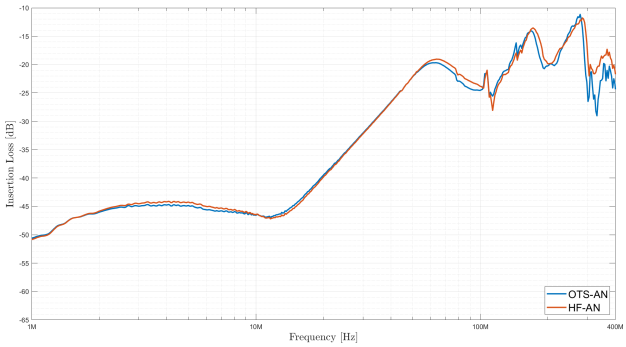

Fig. 13: CM-to-DM conversion in the BCI simulation.

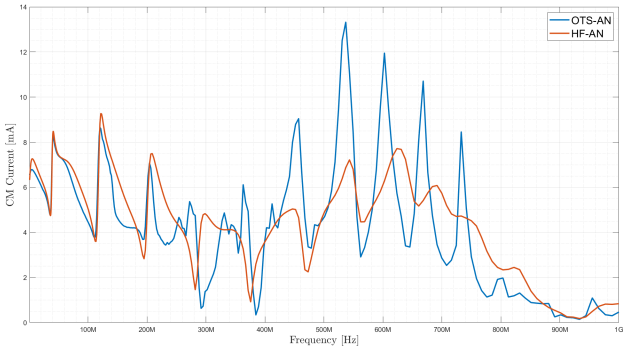

Fig. 14: CM current in the RE simulation.

Fig 12 shows the transimpedance in the CE test setup is barely affected up to 50 MHz. Above that frequency, differences become greater with frequency up to a maximum of 0.6 dB in the positive AN and 3.5 dB in the negative one, leading to overestimations in both cases. Fig 13 shows the BCI situation, in which differences as large as 4.3 dB have been found above 50 MHz. In general, with the HF-AN there were lower insertion losses. Last but not least, Fig 14 shows the RE simulation, in which the CM current was particularly sensitive to the AN impedance. The harness resonances between 300 MHz and 800 MHz showed peaks of 13.30 mA with the OTS-AN while with the HF-AN that peak was of 7.22 mA. This implies that using the OTS-AN instead of the HF-AN has roughly doubled (5.3 dB) the radiated emissions in that band.

V. Discussion

The CISPR 16-1-2 (2017) standard defines the AN impedance up to 108 MHz [20]. This bandwidth does not cover the entire spectrum required in some of the most common EMC situations of the automotive industry like BCI and RE. Despite it is stated in [20] that impedance errors can be considered within the uncertainty budget, this work has demonstrated that the differences can become quantitatively important at high-frequencies. In particular, for RE it was showed on a virtual environment that the emissions profile can be considerably overestimated in the 300 MHz and 800 MHz band if an OTS-AN is used instead of an HF-AN.

As it was stated before, the greatest problem of the OTS-AN is not its mismatch against 50 Ω, but the reproducibility issues the non-RF interfaces can impair. [9] has theoretically demonstrated that the adapters introduce a non-negligible error, sometimes even larger than the measurement uncertainty. Therefore, flexible parts were discouraged in order to improve repeatability and coaxial lines like the ones employed in this work were suggested. In addition to that, in [10], the superior performance of closed adapters in terms of repeatability, reproducibility and accuracy has been showed.

To mitigate these problems, the authors consider the first step is to quantify the test bench by using the “testbench transfer impedance”, which is defined in the ISO 11452-4 (2020) standard as the CM voltage in the injector probe position, divided by the CM current at the measuring probe position [1]. On top of being a fingerprint of the actual testbench, which is significantly useful for comparison among test setups and facilities, it inherently incorporates the effects of the AN. However, as showed by [23], many concerns can be raised regarding the use of it due to the several approximations and high-frequency limitations, especially because important quantities can not be directly derived from it (such as CM-to-DM conversion in BCI, transfer-impedance in CE or CM current in RE). Nevertheless, it is indeed a useful metric for test setups comparisons (given a same set of DUT and load circuit) and we encourage the use of it even in CE and RE, where the probes will have to be added for characterizing the setup signature and then removed. This method looks forward to guaranteeing a better control of the actual test setup conditions.

Last but not least, the OTS-AN exceeds the HF-AN performance when it comes to power handling. The former allows up to 200 A while the latter can only handle 500 mA, due to the current density limitation of the ferrite bead. In terms of battery voltage, the AN can withstand 1000 V while the HF-AN only allows 50 V due to the dielectric strength of the DC capacitors. On account of that, this OTS solution is excessive

for LV and LP applications, while at the same time its non-RF interfaces negatively affect the quantities to be measured.

VI. Conclusions

In the present work, the impedance of a OTS-AN and a custom HF-AN were analysed. Results have demonstrated the importance of using a HF-AN that meets the impedance requirements on the entire bandwidth of the System-level EMC tests. Even though the CISPR 16-1-2 (2017) standard defines the AN impedance, it does not cover the entire bandwidth required for tests like BCI (400 MHz) or RE (1 GHz) as it is only defined up to 108 MHz [20].

It was showed that the impact of using the OTS-AN, when compared to the HF-AN, can lead up to 3.5 dB differences on CE, 4.3 dB on BCI and up to 5.3 dB on RE. Although these quantitative results are highly-dependent on the particular case-studies, the proof of concept is completely applicable to any situation. Therefore, the authors remark not only the importance of considering the actual AN properties for accurate simulations, but also as a source of non-constant uncertainty, specially when non-RF interfaces are used.

In order to consider these effects and mitigate discrepancies, the authors recommend the use of the testbench transfer impedance defined in [1] as a fingerprint of the test setup. Otherwise, the AN effects can be directly translated into a lack of accuracy during the early-design stage simulations as well as a lack of inter-laboratory correlation.

The authors believe nowadays EMC requirements are demanding the trade-offs of the AN design to be reconsidered. Specially for LV and LP applications where the OTS solutions may be excessive for some specifications (like DC current and DC voltage) while at the same time, detrimental in their RF performance.

Acknowledgments

Eduardo Mariani is an exclusive consultant of Allegro MicroSystems Argentina. The authors would like to thank Andrés Altieri for his support with the EM simulations.

References

[1] ISO 11452-4 (2020): Road Vehicles-Component Test Methods for Electrical Disturbances by Narrowband Radiated Electromagnetic Energy Part 4: Bulk Current Injection (BCI), Ed. 5

[2] CISPR 25 (2016): Vehicles, boats and internal combustion engines - Radio disturbance characteristics - Limits and methods of measurement for the protection of on-board receivers, Ed. 4

[3] IEC 62132-4, "Integrated circuits - Measurement of Electromagnetic Immunity 150 kHz to 1 GHz - Part 4: Direct RF power injection method", Ed. 1, 2006

[4] IEC 61967-4, "Integrated Circuits - Measurements of Electromagnetic Emission, 150 kHz to 1 GHz — Part 4: Measurement of Conducted emission - $1\Omega/150\Omega$ Direct Coupling Method", Ed. 1.1, 2006

[5] H. Pues et al., "Translation of automotive module RF immunity test limits into equivalent IC test limits using S-parameter IC models," 2013 9th International Workshop on Electromagnetic Compatibility of Integrated Circuits (EMC Compo), 2013, pp. 249-253, doi: 10.1109/EMCCompo.2013.6735209.

[6] Y. Kondo, M. Izumichi and O. Wada, "Simulation of Bulk Current Injection Test for Automotive Components Using Electromagnetic Analysis," in IEEE Transactions on Electromagnetic Compatibility, vol. 60, no. 4, pp. 866-874, Aug. 2018, doi: 10.1109/TEMC.2017.2751580.

[7] S. Miropolsky, A. Sapadinsky and S. Frei, "A generalized accurate modelling method for automotive bulk current injection (BCI) test setups up to 1 GHz," 2013 9th International Workshop on Electromagnetic Compatibility of Integrated Circuits (EMC Compo), Nara, 2013, pp. 63-68, doi: 10.1109/EMCCompo.2013.6735174.

[8] A. Radchenko et al., "Transfer Function Method for Predicting the Emissions in a CISPR-25 Test-Setup," in IEEE Transactions on Electromagnetic Compatibility, vol. 56, no. 4, pp. 894-902, Aug. 2014, doi: 10.1109/TEMC.2013.2297303.

[9] F. Ziadé et al., "Improvement of LISN Measurement Accuracy Based on Calculable Adapters," in IEEE Transactions on Instrumentation and Measurement, vol. 65, no. 2, pp. 365-377, Feb. 2016, doi: 10.1109/TIM.2015.2479107.

[10] C. Carobbi, D. Passalacqua and G. Basso, "LISN calibration up to 400 MHz," 2019 Kleinheubach Conference, 2019, pp. 1-4.

[11] C. F. M. Carobbi and M. Stecher, "The Effect of the Imperfect Realization of the Artificial Mains Network Impedance on the Reproducibility of Conducted Emission Measurements," in IEEE Transactions on Electromagnetic Compatibility, vol. 54, no. 5, pp. 986-997, Oct. 2012, doi: 10.1109/TEMC.2012.2196046.

[12] C. F. M. Carobbi, "Quantification of the artificial mains network impedance contribution to the uncertainty of conducted emission measurements," 2020 XXXIIIrd General Assembly and Scientific Symposium of the International Union of Radio Science, 2020, pp. 1-4, doi: 10.23919/URSIGASS49373.2020.9232272.

[13] O. Aiello, P. S. Crovetti and F. Fiori, "Susceptibility to EMI of a Battery Management System IC for electric vehicles," 2015 IEEE International Symposium on Electromagnetic Compatibility (EMC), 2015, pp. 749-754, doi: 10.1109/ISEMC.2015.7256257.

[14] O. Aiello and P. Crovetti, "Characterization of the Susceptibility to EMI of a BMS IC for Electric Vehicles by Direct Power and Bulk Current Injection," in IEEE Letters on Electromagnetic Compatibility Practice and Applications, doi: 10.1109/LEMCPA.2021.3085765.

[15] H. Hackl, M. Ibel, B. Auinger, D. List and C. Stockreiter, "Non-Destructive Modeling of a 9V Alkaline Battery for EMC Simulation Based on S-Parameter Measurement," 2020 International Symposium on Electromagnetic Compatibility - EMC EUROPE, 2020, pp. 1-6, doi: 10.1109/EMCEUROPE48519.2020.9245760.

[16] M. Raya and R. Vick, "A simulation method to determine the RF impedance of batteries," 2017 International Symposium on Electromagnetic Compatibility - EMC EUROPE, 2017, pp. 1-5, doi: 10.1109/EMCEurope.2017.8094758.

[17] T. F. Landinger, G. Schwarzberger and A. Jossen, "A Novel Method for High Frequency Battery Impedance Measurements," 2019 IEEE International Symposium on Electromagnetic Compatibility, Signal and Power Integrity (EMC+SIPI), 2019, pp. 106-110, doi: 10.1109/ISEMC.2019.8825315.

[18] S. Pignari and F. G. Canavero, "Theoretical assessment of bulk current injection versus radiation," in IEEE Transactions on Electromagnetic Compatibility, vol. 38, no. 3, pp. 469-477, Aug. 1996, doi: 10.1109/15.536077.

[19] Clayton A. Paul. Introduction to Electromagnetic Compatibility, Second Edition, Wiley, 2006

[20] CISPR 16-1-2 (2017): Specification for radio disturbance and immunity measuring apparatus and methods – Part 1-2: Radio disturbance and immunity measuring apparatus – Coupling devices for conducted disturbance measurements, Ed. 2

[21] Y. Kondo, M. Izumichi, K. Shimakura, O. Wada, "Modeling of Bulk Current Injection Setup for Automotive Immunity Test Using Electromagnetic Analysis," IEICE Trans. Commun., Vol.E98-B, No.07, July, 2015

[22] A. Kriz, "Characterization and correction of calibration jigs for LISN impedance measurements," 2015 IEEE Symposium on Electromagnetic Compatibility and Signal Integrity, 2015, pp. 215-219, doi: 10.1109/EMCSI.2015.7107688.

[23] P. S. Crovetti and F. Fiori, "A Critical Assessment of the Closed-Loop Bulk Current Injection Immunity Test Performed in Compliance With ISO 11452-4," in IEEE Transactions on Instrumentation and Measurement, vol. 60, no. 4, pp. 1291-1297, April 2011, doi: 10.1109/TIM.2010.2084870.